Inorg. Chem. **2007**, *46*, 11437–11449

Testing if the Interstitial Atom, X, of the Nitrogenase Molybdenum–Iron Cofactor Is N or C: ENDOR, ESEEM, and DFT Studies of the $S = {}^3/_2$ Resting State in Multiple Environments

Dmitriy Lukoyanov,[†] Vladimir Pelmenschikov,[‡] Nathan Maeser,[§] Mikhail Laryukhin,[†] Tran Chin Yang,[†] Louis Noodleman,[‡] Dennis R. Dean,[||] David A. Case,[‡] Lance C. Seefeldt,[§] and Brian M. Hoffman*,[†]

Department of Chemistry, Northwestern University, 2145 N. Sheridan Road, Evanston, Illinois 60208-3113, Department of Molecular Biology, The Scripps Research Institute, 10550 North Torrey Pines Road, La Jolla, California 92037, Department of Chemistry and Biochemistry, Utah State University, 0300 Old Main Hill, Logan, Utah 84322-0300, and The Department of Biochemistry, Virginia Polytechnic Institute and State University, Blacksburg, Virginia 24061-0002

Received September 21, 2007

A high-resolution (1.16 Å) X-ray structure of the nitrogenase molybdenum–iron (MoFe) protein revealed electron density from a single N, O, or C atom (denoted **X**) inside the central iron prismane ([6Fe]) of the [$MoFe_7S_9$:homocitrate] FeMo-cofactor (FeMo-co). We here extend earlier efforts to determine the identity of **X** through detailed tests of whether **X** = N *or* C by interlocking and mutually supportive 9 GHz electron spin echo envelope modulation (ESEEM) and 35 GHz electron–nuclear double resonance (ENDOR) measurements on $^{14/15}$N and $^{12/13}$C isotopomers of FeMo-co in three environments: (i) incorporated into the native MoFe protein environment; (ii) extracted into *N*-methyl formamide solution; and (iii) incorporated into the NifX protein, which acts as a chaperone during FeMo-co biosynthesis. These measurements provide powerful evidence that **X** ≠ N/C, unless **X** in effect is magnetically decoupled from the $S = {}^3/_2$ electron spin system of resting FeMo-co. They reveal no signals from FeMo-co in any of the three environments that can be assigned to **X** from *either* $^{14/15}$N or ^{13}C: If **X** were either element, its maximum *observed* hyperfine coupling at all fields of measurement is estimated to be $A(^{14/15}N_X) < 0.07/0.1$ MHz, $A(^{13}C_X) < 0.1$ MHz, corresponding to intrinsic couplings of about half these values. In parallel, we have explicitly calculated the hyperfine tensors for **X** = $^{14/15}$N/^{13}C/^{17}O, nuclear quadrupole coupling constant e^2qQ for **X** = ^{14}N, and hyperfine constants for the Fe sites of $S = {}^3/_2$ FeMo-co using density functional theory (DFT) in conjunction with the broken-symmetry (BS) approach for spin coupling. If **X** = C/N, then the decoupling required by experiment strongly supports the "BS7" spin coupling of the FeMo-co iron sites, in which a small **X** hyperfine coupling is the result of a precise balance of spin density contributions from three spin-up and three spin-down (3↑:3↓) iron atoms of the [6Fe] prismane "waist" of FeMo-co; this would rule out the "BS6" assignment (4↑:2↓ for [6Fe]) suggested in earlier calculations. However, even with the BS7 scheme, the hyperfine couplings that would be observed for **X** near g_2 are sufficiently large that they should have been detected: we suggest that the experimental results are compatible with **X** = N only if $a_{iso}(^{14/15}N_X) < 0.03–0.07/0.05–0.1$ MHz and $a_{iso}(^{13}C_X) < 0.05–0.1$ MHz, compared with calculated values of $a_{iso}(^{14/15}N_X) = 0.3/0.4$ MHz and $a_{iso}(^{13}C_X) = 1$ MHz. However, the DFT uncertainties are large enough that the very small hyperfine couplings required by experiment do not necessarily rule out **X** = N/C.

1. Introduction

Nitrogenase reduces N≡N to two NH_3 molecules under atmospheric pressure and ambient temperature in a reaction coupled to the hydrolysis of MgATP.[1,2] This enzyme has two components, the electron-transfer Fe protein and the molybdenum−iron (MoFe) protein, which contains the active-site metal cluster, the [$MoFe_7S_9$:homocitrate] FeMo-cofactor (FeMo-co). A high-resolution (1.16 Å) X-ray crystallographic study of the MoFe protein revealed electron density from an atom (denoted **X**) inside the central iron prismane ([6Fe]) of FeMo-co at a distance of ∼2.0 Å from

* To whom correspondence should be addressed. E-mail: bmh@northwestern.edu.
[†] Northwestern University.
[‡] The Scripps Research Institute.
[§] Utah State University.
[||] Virginia Polytechnic Institute and State University.

10.1021/ic7018814 CCC: $37.00
Published on Web 11/21/2007

Chart 1

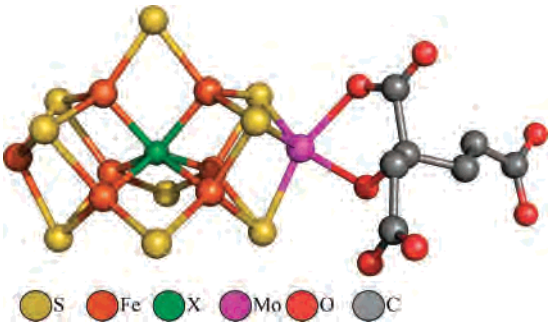

the six trigonal-prismatic irons and ~3.3 Å from all of the sulfur atoms (Chart 1).[3] The electron density associated with **X** is consistent with a single N, O, or C atom, and it was natural to suggest that **X** is an N atom that derives from N_2, possibly exchanging during catalysis. An **X** = N assignment has been favored by many theoretical studies, based on computed geometries and redox potentials.[4−14]

To test whether **X** = N, we carried out a series of $^{14/15}$N electron−nuclear double resonance (ENDOR) and ^{14}N electron spin echo envelope modulation (ESEEM) measurements on the $S = {}^3/_2$ resting state of FeMo-co in the MoFe protein. Earlier ^{14}N ESEEM and ^{15}N ENDOR studies of the MoFe protein had detected two hyperfine-coupled nitrogen atoms, N1 (intrinsic isotropic coupling to $S = {}^3/_2$ spin system, $a_{iso}(^{14}N1) = 1.05$ MHz and $e^2qQ(^{14}N1) = 2.17$ MHz) and N2 ($a_{iso}(^{14}N2) = 0.5$ MHz and $e^2qQ(^{14}N2) = 3.5$ MHz).[15] On the basis of amino acid substitution experiments, these were assigned to nitrogen atoms of α-359^{Arg} (N1) and α-356/357^{Gly} (N2) interacting with FeMo-co. Subsequent ESEEM and ENDOR studies performed in parallel on FeMo-co bound to ($^{14/15}$N) MoFe protein and FeMo-co extracted into *N*-methyl formamide (NMF) from ($^{14/15}$N) MoFe protein first provided evidence that *if* **X** = N, then it is not exchangeable during turnover.[16] They next provided evidence that **X** ≠ N: All the $^{14/15}$N signals from the MoFe protein detected in 35 GHz ENDOR and in 9 and 35 GHz ESEEM studies were shown to come from nitrogen nuclei of the polypeptide, none from the cofactor itself, and none was seen from cofactor extracted into NMF.[17] In addition, a 35 GHz ENDOR signal assigned to natural-abundance ^{13}C was detected and was noted to have a number of possible assignments, including an assignment to **X**.[17] However, subsequent DFT calculations indicated that interstitial atom **X** might have a small net spin population and hence a small hyperfine coupling,[6,18] requiring even more rigorous methods to detect.

To establish whether FeMo-co contains **X** = N *or* C that is hyperfine-coupled to the $S = {}^3/_2$ resting state, we have now performed a complete set of 9GHz ESEEM and 35GHz ENDOR measurements on $^{14/15}$N and $^{12/13}$C isotopomers of FeMo-co in three environments: (i) incorporated into the native MoFe protein environment; (ii) extracted into NMF solution; and (iii) incorporated into the NifX protein, which acts as a chaperone during FeMo-co biosynthesis and which might provide a more ordered environment than that in NMF solution. These experiments address the identity of **X** from two perspectives. Measurements on $^{14/15}$N or $^{12/13}$C isotopomer pairs of FeMo-co in the MoFe protein test whether the protein itself exhibits a signal that cannot be assigned to a site on the polypeptide and must be assigned to **X**; measurements on FeMo-co extracted from isotopomer pairs directly test whether a spin-coupled $^{14/15}$N or ^{13}C is associated with (coextracts with) FeMo-co and thus may be assigned to **X**. These measurements do *not* reveal any signals that can be assigned to **X** from *either* $^{14/15}$N or ^{13}C for FeMo-co in any of the environments and place stringent upper bounds on the possible hyperfine coupling of a proposed **X** = $^{14/15}$N or ^{13}C.

In parallel with these experimental tests of the possibility of detecting interstitial^{14,15}N or ^{13}C, we report the first density functional theory (DFT) computations of the hyperfine parameters that might be expected for **X** = ^{13}C/$^{14/15}$N/^{17}O in the resting state of FeMo-co. The possibility that the interstitial atom has a small hyperfine coupling was originally suggested by calculations that gave a small net spin population, 0.02−0.03*e*, for **X** = N.[6,18] We now explicitly calculate the hyperfine coupling tensors for the above **X** candidates using DFT in combination with the broken-symmetry (BS) approach[19] to spin coupling the FeMo-co iron ions. We show an important connection between the spin couplings of six [6Fe] prismane irons and the magnitude of the hyperfine interaction of **X** with the FeMo-co resting state $S = {}^3/_2$ spin. If **X** = N or C, one particular spin-coupling scheme (BS7) is consistent with all the data we analyze, which includes relative energies of the various spin states, hyperfine coupling for **X** = N/C/O, nuclear quadrupole coupling constants e^2qQ for ^{14}N, and hyperfine coupling constants for the seven ^{57}Fe sites.

(1) Burgess, B. K.; Lowe, D. L. *Chem. Rev.* **1996**, *96*, 2983−3011.
(2) Rees, D. C.; Howard, J. B. *Curr. Opin. Chem. Biol.* **2000**, *4*, 559−566.
(3) Einsle, O.; Tezcan, F. A.; Andrade, S. L. A.; Schmid, B.; Yoshida, M.; Howard, J. B.; Rees, D. C. *Science* **2002**, *297*, 1696−1700.
(4) Dance, I. *Chem. Commun.* **2003**, *3*, 324−325.
(5) Hinnemann, B.; Norskov, J. K. *J. Am. Chem. Soc.* **2003**, *125*, 1466−1467.
(6) Lovell, T.; Liu, T.; Case, D. A.; Noodleman, L. *J. Am. Chem. Soc.* **2003**, *125*, 8377−8383.
(7) Vrajmasu, V.; Muenck, E.; Bominaar, E. L. *Inorg. Chem.* **2003**, *42*, 5974−5988.
(8) Hinnemann, B.; Norskov, J. K. *J. Am. Chem. Soc.* **2004**, *126*, 3920−3927.
(9) Huniar, U.; Ahlrichs, R.; Coucouvanis, D. *J. Am. Chem. Soc.* **2004**, *126*, 2588−2601.
(10) Cao, Z. X.; Jin, X.; Zhang, Q. N. *J. Theor. Comput. Chem.* **2005**, *4*, 593−602.
(11) Dance, I. *Inorg. Chem.* **2006**, *45*, 5084−5091.
(12) Noodleman, L.; Lovell, T.; Han, W.-G.; Li, J.; Himo, F. *Chem. Rev.* **2004**, *104*, 459−508.
(13) Schimpl, J.; Petrilli, H., M.; Blochl P., E. *J. Am. Chem. Soc.* **2003**, *125*, 15772−15778.
(14) Kastner, J.; Blochl P. E. *J. Am. Chem. Soc.* **2007**, *129*, 2998−3006.
(15) Lee, H.-I.; Doan, P. E.; Hoffman, B. M. *J. Magn. Reson.* **1999**, *140*, 91−107.
(16) Lee, H.-I.; Benton, P. M. C.; Laryukhin, M.; Igarashi, R. Y.; Dean, D. R.; Seefeldt, L. C.; Hoffman, B. M. *J. Am. Chem. Soc.* **2003**, *125*, 5604−5605.
(17) Yang, T.-C.; Maeser, N. K.; Laryukhin, M.; Lee, H.-I.; Dean, D. R.; Seefeldt, L. C.; Hoffman, B. M. *J. Am. Chem. Soc.* **2005**, *127*, 12804−12805.
(18) Hinnemann, B.; Norskov, J. K. *Top. Catal.* **2006**, *37*, 55−70.
(19) Noodleman, L. *J. Chem. Phys.* **1981**, *74*, 5737−5743.

2. Experimental Section

2.1. Materials and Methods. Materials. All chemicals used were purchased from Sigma-Aldrich (St. Louis, MO) unless stated otherwise. ^{13}C-D-glucose and ^{15}N-urea were obtained from Cambridge Isotopes (Andover, MA). Nitrogenase Fe and MoFe proteins were expressed from the appropriate strain of *Azotobacter vinelandii*: DJ995 (wild-type (WT) MoFe protein), DJ1313 (α-70^{Gly} MoFe protein), or DJ884 (wild-type Fe protein). Fe and MoFe proteins were purified to homogeneity as previously described.[20] All NMF was vacuum distilled following overnight stirring with a saturating amount of sodium bicarbonate. Na_2HPO_4 was subsequently added to the NMF to a concentration of 2.4 mM.

FeMo-co. Extraction of FeMo-co from MoFe protein was performed using the original procedure of Shah and Brill.[21] Following extraction, the resulting solution was concentrated using a vacuum distillation apparatus to a concentration of approximately 1 mM of FeMo-co in NMF. The integrity of the NMF-isolated FeMo-co was verified by the restoration of acetylene reduction activity for an apo-MoFe protein purified from a Δ*nifB* strain of *A. vinelandii*.[20] Acetylene reduction assays were performed according to previously published methods.[20] When used, thiophenol was added to the isolated FeMo-co solution to an approximate final concentration of 10 μM.

Isotopic Labeling. For convenience, we shall denote FeMo-co according to the isotopic composition of the MoFe protein from which it was labeled; for example, (^{15}N) FeMo-co is isolated from (^{15}N) MoFe protein.

^{13}C-labeled MoFe protein was purified from DJ995 cells grown on media containing a minimal amount (5 g/L) of D-glucose as the sole carbon source. Five percent of the total glucose by weight was ^{13}C-D-glucose (99% ^{13}C) with the remaining 95% being natural-abundance D-glucose (1% ^{13}C).

MoFe protein labeled with ^{15}N was purified from an *A. vinelandii* strain containing a MoFe protein (α-70^{Gly} MoFe protein) that is incapable of dinitrogen fixation (DJ1313). Therefore, all nitrogen incorporated into the protein was derived from ^{15}N-urea (98+% ^{15}N) added to the growth media to a final concentration of 0.83 mM.

Expression and Purification of *nifX*. A plasmid containing the *nifX* gene cartridge, pDB553, was used to express the NifX protein in *E. coli* strain BL21 (DE3). The BL21 cells, transformed with pDB553, were grown at 30 °C on LB media containing 100 μg/mL ampicillin, and the expression of NifX was induced by the addition of 1% (w/v) lactose to the growth medium followed by 2 h of induction. The cell were then collected by centrifugation and frozen at −80 °C.

For purification of NifX, the cells were suspended in 25 mM Tris buffer, pH 7.4, using 2 mL of buffer per 1 g of wet cell paste. The cells were disrupted by sonication, followed by the addition of 1% (w/v) of streptomycin sulfate. After an incubation period of 5 min at 25 °C, the disrupted cells were centrifuged for 1 h at 20 000*g*. Ammonium sulfate was then added to the crude extract supernatant to a final concentration of 40% of saturation and allowed to stir for 5 min. The sample was then centrifuged 30 min at 10 000*g*. The supernatant was again collected, and additional ammonium sulfate was added, bringing the solution to 50% of saturation. The sample was again centrifuged for 30 min at 10 000*g*, with the precipitated protein being collected. The protein pellet, containing a majority of NifX, was then suspended in 30 mL of 25 mM Tris buffer, pH 7.4. This solution was loaded onto a Q-sepharose column and eluted using a 200 mL gradient volume (0.1−0.6 M) of NaCl. Fractions were collected in degassed vials, and the presence of NifX was detected by SDS-PAGE with Coomassie blue staining. Those fractions containing a large amount of NifX were pooled and concentrated by ultrafiltration. Purified NifX was frozen in liquid nitrogen.

Binding of FeMo-co to NifX was performed by first diluting the NifX with a 200 mM potassium phosphate buffer, pH 7.3, containing 2 mM sodium dithionite. The final diluted volume was selected such that, upon the addition of a slight excess of FeMo-co, the concentration of NMF would not exceed 2% by volume. Incubation was performed in a sealed serum vial under argon at 25 °C for 10 min with gentle stirring. Following this incubation period, the resulting NifX-FeMo-co solution was concentrated to a final approximate concentration of 3 mM (or 51 mg/mL) by ultrafiltration.

2.2. Spectroscopy. Electron Paramagnetic Resonance (EPR)/ENDOR Spectroscopy. The spectrometers previously described were used to record CW EPR spectra[22] and pulsed 35 GHz ENDOR spectra;[23] ENI A500 and AMT M3445 amplifiers were used for the ENDOR measurements. EPR spectra obtained at 2 K in dispersion mode under "rapid-passage" conditions give an absorption line shape.[24] The Davies pulse sequence, [π-T(rf)-π/2-τ-π-detect], was used when searching for signals with large hyperfine couplings; the Mims pulse sequence, [π/2-τ-π/2-T(rf)-π/2-detect], was used when collecting spectra from nuclei with smaller couplings, $A < 5$ MHz.[25] The ENDOR pattern for $I = {}^1/_2$ nucleus (^{13}C, ^{15}N) exhibits a $\nu(\pm)$ doublet that is split by the hyperfine coupling, A, and centered at the nuclear Larmor frequency. The Mims pulse sequence has the property that its ENDOR intensities follow the relationship

$$I(A\tau) \sim 1 - \cos(2\pi A\tau) \tag{1}$$

According to this function the intensity is nulled when $A\tau = 0$, 1, 2, ...n and "blind spots" appear in ENDOR spectrum; when $A\tau = n + {}^1/_2$, the intensity should maximize.[25] To compare intensities from ^{13}C-enriched and natural-abundance samples, each ^{13}C spectrum was normalized to the spin echo height of that sample and normalized for the number of scans.

X-band three-pulse ESEEM[25] timewaves were collected at 4.5 K on a Bruker ElexSys E-580 FT-EPR spectrometer equipped with an Oxford ESR-9 cryostat. The timewaves were Fourier transformed to give frequency-domain (ENDOR-like) spectra through the use of Bruker *Xepr* software.

EPR and ENDOR Analysis. The ENDOR patterns for nuclei with spins $I = {}^1/_2$, 1, are given to first order by

$$\nu_{\pm} = |\nu_n \pm A/2| \quad (I = 1/2) \tag{2a}$$

$$\nu_{\pm\pm} = |\nu_n \pm A/2 \pm 3P/2| \quad (I = 1) \tag{2b}$$

where ν_n is the nuclear Larmor frequency, A is the orientation-dependent hyperfine coupling constant, and P is the orientation-dependent quadrupole interaction; exact solutions for $I = 1$, which

(20) Christiansen, J.; Goodwin, P. J.; Lanzilotta, W. N.; Seefeldt, L. C.; Dean, D. R. *Biochemistry* **1998**, *37*, 12611−12623.
(21) Shah, V. K.; Brill, W. J. *Proc. Natl. Acad. Sci. U.S.A.* **1977**, *74*, 3249−3253.
(22) Werst, M. M.; Davoust, C. E.; Hoffman, B. M. *J. Am. Chem. Soc.* **1991**, *113*, 1533−1538.
(23) Davoust, C. E.; Doan, P. E.; Hoffman, B. M. *J. Magn. Reson.* **1996**, *119*, 38−44.
(24) Mailer, C.; Taylor, C. P. S. *Biochim. Biophys. Acta* **1973**, *322*, 195−203.
(25) Schweiger, A.; Jeschke, G. *Principles of Pulse Electron Paramagnetic Resonance*; Oxford University Press: Oxford, U.K., 2001.

Chart 2

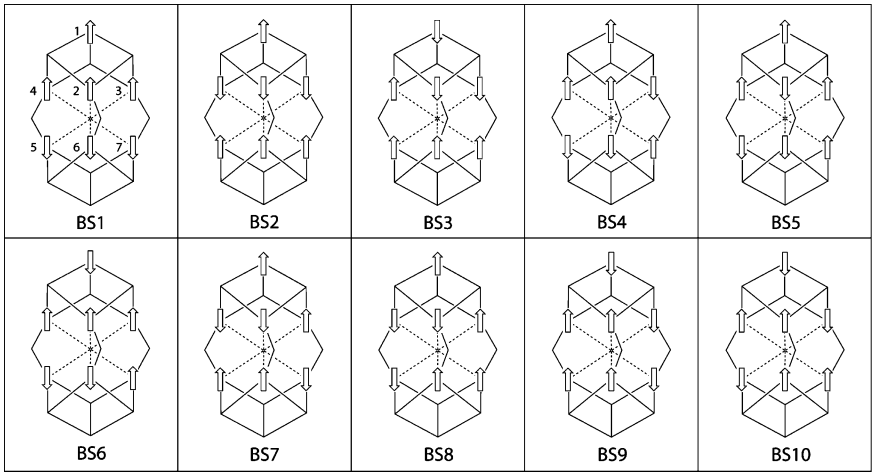

also allow analysis of "double-quantum" transitions are well-known.[26] Full hyperfine tensors were obtained by the simulation of 2D field-frequency patterns comprised of multiple ENDOR spectra taken across the EPR envelope, as described.[27,28] ESEEM timewaves were simulated with a program kindly provided by Professor Kurt Warncke.

The resting FeMo-co has a true electron spin of $S = {}^3/_2$ that results from exchange interactions among the Fe ions. However, its' EPR signal is treated in terms of a fictitious spin, $S' = {}^1/_2$, with strongly anisotropic **g** tensor, $\mathbf{g} = [g_1, g_2, g_3] \sim [4.3, 3.6, 2]$. In describing the results of ENDOR/ESEEM experiments we must distinguish among several types of hyperfine coupling constants and hyperfine tensors.

(i) A hyperfine interaction and interaction tensor measured as splittings in an ENDOR or ESEEM spectrum of a spin-coupled nucleus correspond to the interaction with the fictitious spin ($S' = {}^1/_2$); they are denoted simply, A and **A**.

(ii) In contrast are hyperfine tensors that correspond to the nuclear interaction with the true spin ($S = {}^3/_2$); these will be denoted ${}^{3/2}A$ and ${}^{3/2}\mathbf{A}$. The isotropic couplings derived either from experiment or calculated theoretically are defined only relative to and always refer to the true $S = {}^3/_2$ spin; as a shorthand, we will write them as a_{iso}, suppressing the ${}^3/_2$ label.

(iii) Finally, the observed ($S' = {}^1/_2$) couplings are strongly modified from the hyperfine couplings expressed relative to the true $S = {}^3/_2$ electron spin. For example, if the **g** and $S = {}^3/_2$ hyperfine tensor, ${}^{3/2}\mathbf{A}$, are coaxial, then the $S' = {}^1/_2$ (measured) hyperfine parameters are given by

$$\mathbf{A} = [(g_1/g_e)\,{}^{3/2}A_1, (g_2/g_e)\,{}^{3/2}A_2, (g_3/g_e)\,{}^{3/2}A_3] \qquad (3)$$

Thus, even an isotropic hyperfine coupling to the $S = {}^3/_2$ spin system, coupling constant a_{iso}, would manifest itself in the spectra as an axial observed hyperfine tensor, $\mathbf{A} = [(g_1/g_e)\,a_{iso}, (g_2/g_e)\,a_{iso}, (g_3/g_e)\,a_{iso}]$.[28]

2.3. Computational Details. Modeling. The starting geometry for the present molecular modeling of FeMo-co was extracted from 1.16 Å resolution 1M1N PDB file.[3] The model includes the [Mo-7Fe-9S-**X**] core and its' covalent ligands α-275^{Cys}, α-442^{His}, and *R*-homocitrate as methylthiolate, imidazole, and glycolate ($^-OCH_2-COO^-$), respectively. For the cofactor resting state, the model total charge is $-4e$, $-3e$, and $-2e$ for $\mathbf{X} = C^{4-}$, N^{3-}, and O^{2-}. This corresponds to formal oxidation states [$Mo^{4+}3Fe^{3+}4Fe^{2+}$] for the metals. Arguments in favor of this charge model have been given elsewhere[6,7,29] and are based on comparisons of experimental and computed Mössbauer isomer shifts, geometries, and redox potentials.

Density Functional Methods. The calculations were done using the parametrization of electron gas data given by Vosko, Wilk, and Nusair (VWN, formula version V)[30] for the local density approximation and the corrections proposed in 1991 by Perdew and Wang (PW91)[31] for the generalized gradient approximation, as implemented in the Amsterdam Density Functional (ADF)[32] package. During the geometry optimizations by ADF, triple-ζ plus polarization (TZP) basis sets were used for Fe and Mo metal sites, while double-ζ plus polarization (DZP) basis sets were used for everything else. The inner shells of Fe($1s^22s^22p^6$) and Mo($1s^22s^2-2p^63s^23p^64s^23d^{10}$) were treated by the frozen core approximation. Single point wave functions, used to report the properties (relative energies, spin densities and spin populations, hyperfine couplings), were obtained using the TZP basis set on all the atoms, with the frozen core used only for Mo as described above. For all the calculations including geometry optimizations, effects of the polar protein environment were considered using the conductor-like screening model (COSMO)[33−36] with the dielectric constant set to $\epsilon = 4.0$.

BS States. FeMo-co of nitrogenase includes eight metal sites, and a spin configuration satisfying $S = {}^3/_2$ total spin for the resting M^N state is by no means unique. Assuming [$Mo^{4+}3Fe^{3+}4Fe^{2+}$] for the formal valencies, a combinatorial search through the simple collinear spin-coupling model for three high-spin ferric (Fe^{3+}, d^5,

(26) Muha, G. M. *J. Chem. Phys.* **1980**, *73*, 4139−4140.
(27) DeRose, V. J.; Hoffman, B. M. In *Methods in Enzymology*; Sauer, K., Ed.; Academic Press: New York, 1995; Vol. 246, pp 554−589.
(28) Hoffman, B. M.; DeRose, V. J.; Doan, P. E.; Gurbiel, R. J.; Houseman, A. L. P.; Telser, J. *Biol. Magn. Reson.* **1993**, *13 (EMR of Paramagnetic Molecules*), 151−218.
(29) Yoo, S. J.; Angove, H. C.; Papaefthymiou, V.; Burgess, B. K.; Muenck, E. *J. Am. Chem. Soc.* **2000**, *122*, 4926−4936.
(30) Vosko, S. H.; Wilk, L.; Nusair, M. *Can. J. Phys.* **1980**, *58*, 1200−1211.
(31) Perdew, J. P.; Chevary, J. A.; Vosko, S. H.; Jackson, K. A.; Pederson, M. R.; Singh, D. J.; Fiolhais, C. *Phy. Rev. B: Condens. Matter Mater. Phys.* **1992**, *46*, 6671−6687.
(32) Te Velde, G.; Bickelhaupt, F. M.; Baerends, E. J.; Fonseca Guerra, C.; Van Gisbergen, S. J. A.; Snijders, J. G.; Ziegler, T. *J. Comput. Chem.* **2001**, *22*, 931−967.
(33) Pye, C.; Ziegler, T. *Book of Abstracts*, 218th National Meeting of the American Chemical Society, New Orleans, LA, Aug 22−26, 1999; American Chemical Society: Washington, DC, 1999; U337−U337.
(34) Klamt, A.; Jonas, V. *J. Chem. Phys.* **1996**, *105*, 9972−9981.
(35) Klamt, A. *J. Phys. Chem.* **1995**, *99*, 2224−2235.
(36) Klamt, A.; Schueuermann, G. *J. Chem. Soc., Perkin Trans. 2* (*1972−1999*) **1993**, 799−805.

Table 1. Mulliken Spin Populations ρ(Fe), Assigned Oxidation States, Site Spins S_i, Derived Spin Projection Coefficients K_i, Semiempirical Fe Hyperfine Couplings a_i^{calc} for FeMo-co Irons, Spin Coupling BS7, and M^N State[a]

Fe$_i$	ρ(Fe$_i$) (e)	oxidation state	S_i	K_i	a_i^{calc} (MHz)	a_i^{exp} (MHz)	site type
1	2.91	2.5+	9/4	+3/10	−6.3	−11.8	A^3
2	−2.60	3+	5/2	−2/5	+6.4	+11.7	B^1
3	2.84	2.5+	9/4	+3/10	−6.2	−3.7	A^4
4	−2.61	3+	5/2	−2/5	+6.5	+11.7	B^1
5	2.41	2+	2	+1	−20.5	−17.1	A^2
6	2.40	2+	2	+1	−20.4	−18.0	A^1
7	−2.55	2+	2	−4/5	+17.3	+9.3	B^2
sum				+1	−23.1	−17.9	

[a] The matching experimental hyperfine couplings[29] and spectroscopic sites are given in the last two columns.

$S = {}^5/_2$) and four high-spin ferrous (Fe^{2+}, d^6, $S = 2$) sites results in the 10 possible spin alignments[37] shown in Chart 2; (the distinct rotamers of the pseudo-C_3 symmetry [Mo-7Fe-9S-**X**] core are omitted here.) All the BS alignments have a 4↑:3↓ spin-coupling pattern. Because these spin orderings do not represent pure spin states but rather BS states,[19] the nomenclature BS1 to BS10 was originally applied. When using ADF, a desired BS state was achieved by first converging the ferromagnetic high-spin (7↑, HS) state ($S = {}^{31}/_2$ for [$Mo^{4+}3Fe^{3+}4Fe^{2+}$]), then exchanging α and β electron densities associated with the three spin-down (3↓) Fe atoms, and finally restarting and converging the calculation, including both self-consistent field and geometry optimization.

Calculation of the Hyperfine Coupling Parameters for Fe and for X. Hyperfine coupling $\boldsymbol{A}$ tensors were calculated based on electronic spin densities obtained from ADF.[38] The isotropic contribution a_{iso}^{UBS} to the calculated unrestricted broken symmetry (UBS) ("raw") $\boldsymbol{A}$ tensor, also called the Fermi or contact interaction, is proportional to the point electron spin density, $|\Psi(0)|^2$, at the nucleus,

$$a_{iso}^{UBS} = (8\pi/3h)\cdot g_e\beta_e g_N\beta_N\cdot|\Psi(0)|^2/2S_t \qquad (4)$$

where S_t is the total electron spin of the system. In case of an **X** atom confined within [6Fe] prismane of FeMo-co, this raw result must be projected onto the total system spin. Quantitatively, this can be expressed as follows:[39,40]

$$a_{iso}(\mathbf{X}) = {}^1/_6 \sum_{i=2,3...7} (|K_i/S_i|S_t)a_{iso}^{UBS}(\mathbf{X}) = P_x a_{iso}^{UBS}(\mathbf{X}) \qquad (5)$$

where $a_{iso}(\mathbf{X})$ is the calculated spin-coupled isotropic hyperfine parameter, which can be compared to experiment; the sum is over the prismatic Fe sites neighboring **X**. The complete $A(\mathbf{X})$ tensor is evaluated from $A^{UBS}(\mathbf{X})$ in an analogous fashion. Here, K_i is a spin projection coefficient of the ith Fe atom of FeMo-co, giving the projection of the local Fe site spin S_i onto the total system spin S_t

$$K_i = \langle \boldsymbol{S}_i\cdot\boldsymbol{S}_t\rangle/\langle \boldsymbol{S}_t\cdot\boldsymbol{S}_t\rangle \qquad (6)$$

A calculation of the K_i factors has been done earlier[37] for the case of [$Mo^{4+}Fe^{3+}6Fe^{2+}$] FeMo-co, $S_t = {}^3/_2$, BS6. The analogous approach for [$Mo^{4+}3Fe^{3+}4Fe^{2+}$] is used here. The individual Fe site spins S_i were assigned based on BS7 state ρ(Fe$_i$) Mulliken spin populations to either ${}^5/_2$ (Fe^{3+}), ${}^9/_4$ (mixed valence $Fe^{2.5+}$), or 2 (Fe^{2+}) (see Table 1). Parallel or antiparallel spin vector alignments were used for composite spins:

$$S_{13} = S_1 + S_3 = {}^9/_2$$

$$S_{24} = S_2 + S_4 = 5$$

$$S_{56} = S_5 + S_6 = 4$$

$$S_{cubane} = S_{1234} = |S_{13} - S_{24}| = {}^1/_2$$

$$S_{triangle} = S_{567} = |S_{56} - S_7| = 2$$

$$S_t = S_{1234567} = |S_{triangle} - S_{cubane}| = {}^3/_2$$

The K_i values to be used in eq 5 were obtained by applying spin projection chain and sum rules[37,39] and are given in Table 1. A final scaling factor $P_{\mathbf{X}} = 0.46$ was obtained for $a_{iso}(\mathbf{X})$, which was used to calculate all the hyperfine couplings reported in the text. However, it is also possible to have "canted" spin alignments, where pairwise couplings are neither fully ferromagnetic nor fully antiferromagnetic. One well-known example of this occurs in [4Fe4S] clusters in high-potential iron proteins.[41] If such canted couplings were present in FeMo-co, the effective $P_{\mathbf{X}}$ value might differ from that used here; furthermore, $P_{\mathbf{X}}$ varies with the choice of BS state (at present it is formulated for BS7). Overall, the value for $a_{iso}^{UBS}(\mathbf{X})$ is the major factor in determining final $a_{iso}(\mathbf{X})$; see eq 5 and Table 4.

Density functional calculations generally provide a poor description of spin densities and Fermi contact couplings at transition-metal nuclei. For this reason, semiempirical calculations for the ^{57}Fe site hyperfine couplings (a_i^{calc}, see Table 1) were performed based on the following equation:

$$a_i^{calc} = K_i(|\rho(Fe_i)|/2S_i)a_i^{ionic} \qquad (7)$$

where typical intrinsic Fe site hyperfine a^{ionic} parameters are[40]

$$a^{ionic}(Fe^{2+}) = -34.0 \text{ MHz}$$

$$a^{ionic}(Fe^{2.5+}) = -32.5 \text{ MHz}$$

$$a^{ionic}(Fe^{3+}) = -31.0 \text{ MHz}$$

This procedure was originally developed to interpret iron hyperfine constants in the P cluster of the MoFe protein, as well as other iron−sulfur proteins[40,42] and is expected to provide a good qualitative picture of how couplings from the individual sites are manifested in the experimental (coupled) spectrum.

3. Experimental Results

We first present the results of EPR/ENDOR/ESEEM experiments on FeMo-co[14,15]N and[12,13]C isotopologs in three environments: MoFe protein, NMF solution, and incorporated into NifX protein (Section 3). Next, we discuss the parallel results from DFT computations (Section 4).

3.1. Q-Band EPR. Figure 1 compares the 2 K absorption-display Q-band rapid passage dispersion-mode EPR spectra[24] of resting-state FeMo-co within the MoFe protein, FeMo-co extracted into NMF, and FeMo-co incorporated into the

(37) Lovell, T.; Li, J.; Liu, T.; Case, D. A.; Noodleman, L. *J. Am. Chem. Soc.* **2001**, *123*, 12392−12410.
(38) van Lenthe, E.; van der Avoird, A.; Wormer, P. E. S. *J. Chem. Phys.* **1998**, *108*, 4783−4796.
(39) Noodleman, L.; Peng, C. Y.; Case, D. A.; Mouesca, J. M. *Coord. Chem. Rev.* **1995**, *144*, 199−244.
(40) Mouesca, J. M.; Noodleman, L.; Case, D. A.; Lamotte, B. *Inorg. Chem.* **1995**, *34*, 4347−4359.
(41) Noodleman, L. *Inorg. Chem.* **1988**, *27*, 3677−3679.
(42) Mouesca, J. M.; Noodleman, L.; Case, D. A. *Inorg. Chem.* **1994**, *33*, 4819−4830.

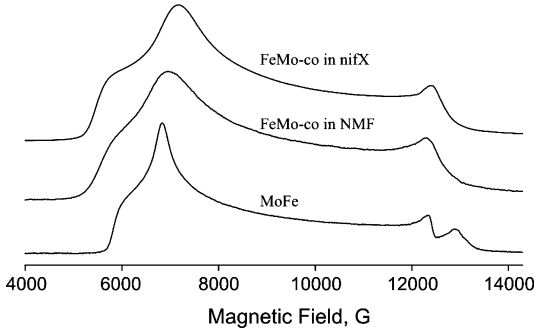

Figure 1. Q-band absorption-display rapid-passage EPR spectra of MoFe protein, extracted FeMo-co, and FeMo-co in *nifX*. Conditions*:* microwave frequency, 34.942−35.038 GHz; microwave power, ∼1 mW; modulation amplitude, 1.3 G; sweep rate, 66 G/sec; time constant, 128 ms; temperature, 2 K.

NifX protein (labeled as "FeMo-co in NifX"). FeMo-co in the MoFe protein shows a well-defined rhombic EPR signal with typical g values (4.32, 3.66, 2.01) arising from the lower Kramer's doublet ($m_s = \pm^1/_2$) of the $S = {}^3/_2$ cofactor state. FeMo-co extracted into NMF gives a comparable but broader signal with altered g values (4.50, 3.59, 2.00). The signal from FeMo-co bound to NifX is sharper than that of FeMo-co in NMF but still broader than that of the enzyme and with altered g values (4.58, 3.49, 1.99). Thus, the protein environment provided by NifX does *not* mimic that of the enzyme. The broadened signals of FeMo-co in NMF and NifX imply that FeMo-co in the nonenzyme environments exhibits a distribution of conformations, in contrast to the well-defined environment of the enzyme.

3.2. ^{14}N ESEEM. (a) (^{14}N) FeMo-co in MoFe. The first evidence regarding the possibility that **X** = N is implicit in earlier ESEEM studies of the $S = {}^3/_2$ state of FeMo-co in the MoFe protein and of the cofactor extracted into NMF, carried out before the existence of **X** was reported.[43] The WT MoFe protein exhibits strong spin−echo modulation (∼90% at g_1), which was analyzed in terms of a hyperfine-coupled nitrogen atom, N1 (a_{iso} = 1.05 MHz and e^2qQ = 2.17 MHz).[15,44] This modulation is eliminated by the α-195$^{His\rightarrow Asn}$ substitution, which reveals weaker modulation (15%) from a second ^{14}N site, which could be completely analyzed in terms of a second hyperfine-coupled nitrogen, N2 (a_{iso} = 0.5 MHz and e^2qQ = 3.5 MHz); the weakly modulating ^{14}N2 has been assigned to α-356/357^{Gly}. Thus, ESEEM from MoFe protein could be wholly assigned without recourse to an additional ^{14}N that might be **X**.

(^{14,15}N) FeMo-co in *nifX*. Figure 2A presents the three-pulse X-band ESEEM timewaves of (^{14,15}N) FeMo-co in NifX, collected at two different fields, g_2 = 3.5 (peak of EPR signal) and g_3 = 2.0. At both fields, the ^{14}N timewaves show modulation with a depth of ∼10% from ^{14}N; the ^{1}H modulation at the field of at g_2 is almost completely suppressed by the choice of τ = 116 ns. Inspection shows no difference between the modulations of the (^{14}N) and (^{15}N) FeMo-co samples; the slight differences in phase memory

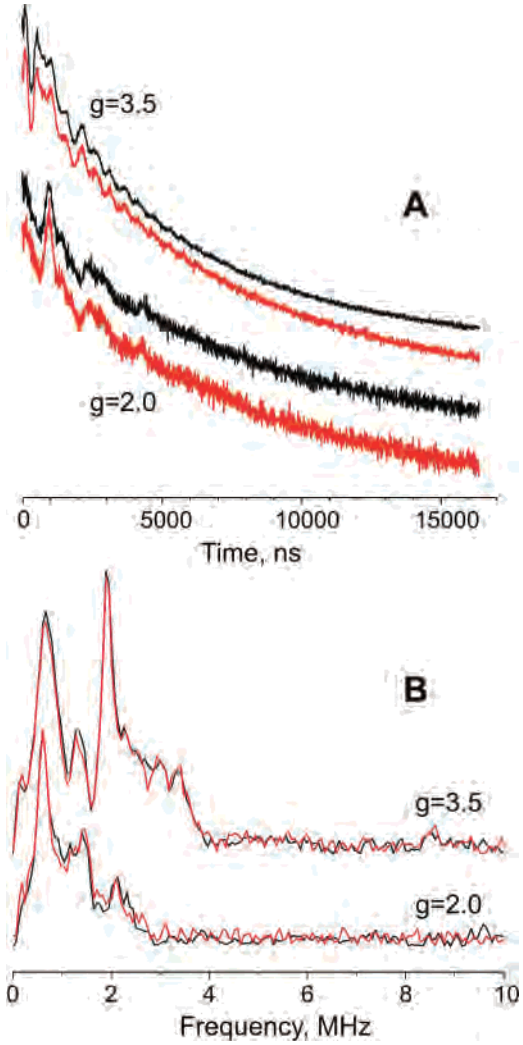

Figure 2. X-band three-pulse ESEEM time-domain (A) and frequency-domain (B) spectra of ^{15}N labeled FeMo-co in nonlabeled (^{14}N) NifX (red) and nonlabeled (^{14}N) FeMo-co in nonlabeled (^{14}N) NifX (black traces). Conditions: microwave frequency, 9.700−9.708 GHz, g = 3.5 and 2.0; $\pi/2$ = 16 ns, τ = 116 ns; temperature, 4.3 K.

at g = 3.5 likely reflect a tiny difference in sample temperatures. Consideration of the signal-to-noise (S/N) ratio of the timewaves indicates that if **X** = N, then the amplitude of its spin echo modulation is below the minimum detectable amplitude set by the noise level, ∼2%. Figure 2B presents the frequency-domain spectra obtained by Fourier transformation of the timewaves. These too show no significant difference. To directly examine any differences between ESEEM responses of ($^{14/15}$N) FeMo-co in NifX, the timewaves of the two isotopomers at each field were divided and the resultant Fourier was transformed. The divided timewave would contain ^{14}N modulation that had been eliminated by isotopic replacement but shows no modulation above the noise level; the transform of the divided timewave likewise shows no peaks above the noise.

The equivalence of the ESEEM responses from ($^{14/15}$N)-FeMo-co in NifX shows that within the stated limits of signal/noise, all the observed ^{14}N ESEEM can be assigned to ^{14}N of NifX. The well-resolved modulation of the ESEEM timewaves and sharp features in the frequency-domain spectra further show that the inhomogeneous broadening of

(43) Thomann, H.; Morgan, T. V.; Jin, H.; Burgmayer, S. J. N.; Bare, R. E.; Stiefel, E. I. *J. Am. Chem. Soc.* **1987**, *109*, 7913−7914.
(44) Lee, H.-I.; Thrasher, K. S.; Dean, D. R.; Newton, W. E.; Hoffman, B. M. *Biochemistry* **1998**, *37*, 13370−13378.

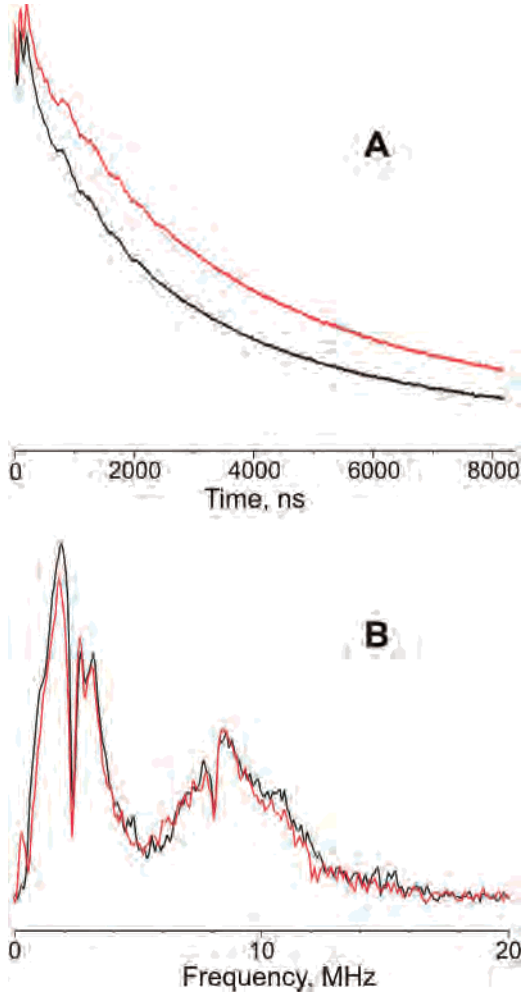

Figure 3. X-band three-pulse ESEEM time-domain (A) and frequency-domain (B) spectra of ^{15}N labeled FeMo-co (red) and nonlabeled (^{14}N) FeMo-co (black traces) extracted in NMF. Conditions: microwave frequency, 9.703−9.705 GHz, $g = 3.6$; $\pi/2 = 16$ ns, $\tau = 116$ ns; temperature, 4.3 K.

the EPR signal is *not* accompanied by inhomogeneous distribution in hyperfine and quadrupole interactions associated with nuclei coupled to the $S = {}^3/_2$ electron spin system. This finding is important for the interpretation of the ENDOR measurements to be discussed below.

($^{14/15}$N) FeMo-co in NMF. Figure 3A presents the three-pulse X-band ESEEM timewaves of ($^{14/15}$N) FeMo-co extracted into NMF, collected at $g_2 = 3.6$; Figure 3B presents the frequency-domain spectra obtained by Fourier transformation of these two timewaves. Once again, the timewave shows distinct modulation, although the modulation depth is lower(~5%) and the frequency-domain spectra are not surprisingly quite different from those of FeMo-co in NifX. However, just as for FeMo-co in NifX, there are no significant differences between the timewaves or frequency-domain spectra of ($^{14/15}$N) FeMo-co in NMF, and the divided timewave exhibits no modulation. Consideration of the S/N ratio of the timewaves again indicates that the ESEEM measurements on extracted FeMo-co in NMF agree with those on FeMo-co in NifX: $S = {}^3/_2$ FeMo-co shows no spin−echo modulation from $\mathbf{X} = {}^{14}$N with a modulation depth of ~2% or greater.

The modulation for FeMo-co in NMF might be from ^{14}N of NMF, but it might also be from ^{23}Na, as the 35 GHz ENDOR measurements described below show coupling to ^{23}Na. Regardless, the well-defined modulation and sharp ESEEM peaks again show that for FeMo-co in NMF, as in NifX, the broadened EPR signal is not accompanied by broad distributions in hyperfine interactions with nuclei coupled to the electron spin.

3.3. ^{14,15}N ENDOR. (b) ^{15}N ENDOR. Figure 4A compares 35GHz Mims pulsed ^{15}N ENDOR spectra collected with $\tau = 500$ ns at $g = 2.0$ from (i) globally labeled α-70^{Gly} (^{15}N)-MoFe protein, (ii) (^{15}N)FeMo-co in natural-abundance (^{14}N)-NifX, and (iii) (^{14}N)FeMo-co in (^{14}N)NifX. Spectra collected at other g values are shown in Figure S1 (Supporting Information). The $g = 2$ spectrum from MoFe protein shows ^{15}N ENDOR signals from two distinct nitrogen nuclei, with hyperfine couplings, $A_1 = 1.6$ MHz and $A_2 = 0.35$ MHz; broader sweeps show there no signals from more strongly coupled ^{15}N. The ^{15}N signals of N1/2 do *not* appear in the ENDOR spectra of FeMo-co in NMF (not shown) or in NifX (Figure 4A). This observation, coupled with the sharp ^{14}N ESEEM peaks seen for FeMo-co in NifX and NMF, indicates that N1/2 do not extract with FeMo-co, thus confirming that they are not associated with **X**. The ENDOR spectra of the FeMo-co in NifX also show a signal at −1.0 MHz relative to the ^{15}N Larmor frequency that is not observed for the MoFe protein or FeMo-co in NMF; as it is seen for both FeMo-co isotopomers we assign it to ^{14}N that is part of the NifX protein.

Figure 5 shows a 2D field-frequency plot comprised of ^{15}N ENDOR spectra collected at multiple fields across the EPR envelope of the (^{15}N)MoFe protein. The field dependence of ^{15}N1 can be simulated with a hyperfine interaction that is essentially isotropic, ${}^{3/2}\mathbf{A}({}^{15}\text{N1}) = [1.45(4), 1.5(4), \text{and } 1.5(4)]$ MHz and ${}^{3/2}a({}^{15}\text{N1})_{iso} = 1.48(4)$ MHz, and that for ^{15}N2 with an interaction that is completely isotropic, ${}^{3/2}a({}^{15}\text{N2})_{iso} = 0.32(4)$ MHz. The corresponding ^{14}N isotropic couplings are $a({}^{14}\text{N1})_{iso} = 1.05$ MHz and $a({}^{14}\text{N2})_{iso} = 0.23$ MHz. The ^{15}N2 doublet splits in spectra collected (roughly) between g_1 and g_2, indicating that the signal comes from two almost identical nitrogen nuclei. Given the assignment of N2 to α-356/357^{Gly}, we may be resolving contributions from the two residues or signals from two different conformations (substates) of the same site. The possibility that this signal represents a fortuitous overlap of a signals from α-356/357^{Gly} and $\mathbf{X} = $ N can be dismissed, as the extracted cofactor shows neither the ^{14}N2 ESEEM nor the ^{15}N2 35 GHz Mims ENDOR signal.

Given the dependence of the Mims ENDOR response to the value of the product, $A\tau$ (eq 1), the absence of ^{15}N pulsed ENDOR signals other than those from N1 and N2 (Figures 4A and 5), which are associated with residues of the MoFe protein, implies that if $\mathbf{X} = $ N, then the ^{15}N hyperfine coupling to $^{15}\mathbf{N_X}$ is too small to have been detected in the spectra taken with $\tau = 500$ ns. To search for possible ^{15}N signal(s) in (^{15}N)MoFe protein with hyperfine coupling(s) smaller than that of ^{15}N2, we collected spectra over narrower sweep and at longer pulse intervals, $\tau \leq 1500$ ns, to enhance

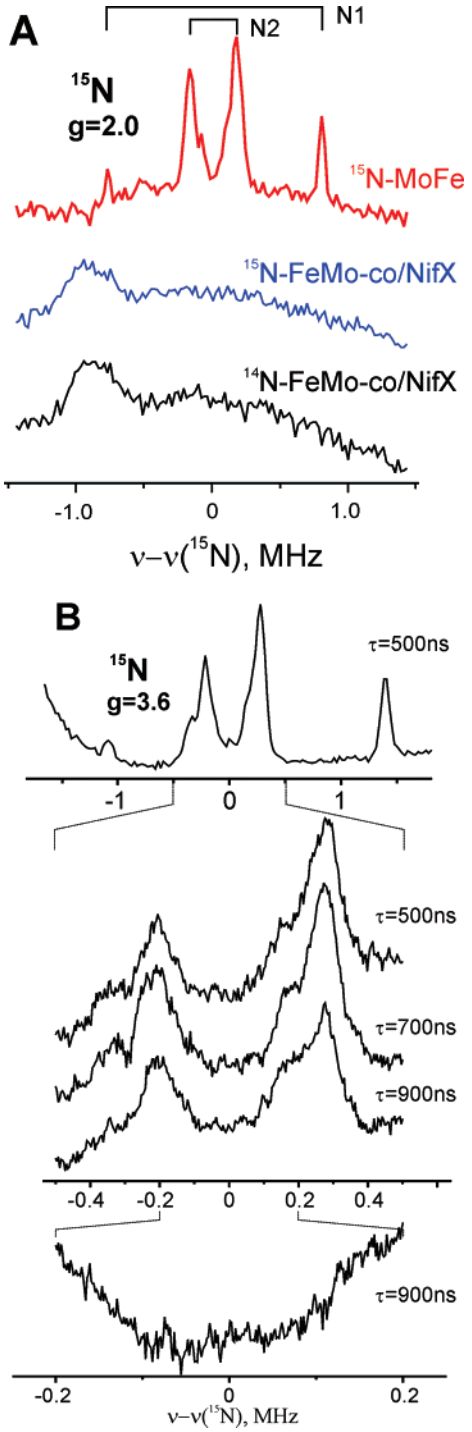

Figure 4. Mims ^{15}N ENDOR spectra. (**A**) NifX (^{15}N) α-70^{Gly} MoFe protein, (^{15}N) FeMo-co in (^{14}N) NifX, and (^{14}N) FeMo-co in (^{14}N) NifX. *Conditions*: microwave frequency, 34.581−34.745 GHz; $g = 2.0$; Mims sequence, $\pi/2 = 52$ ns, $\tau = 500$ ns; radio frequency (RF) = 20 μs; 30 shots/point; repetition time, 10 ms; 50 scans; T = 2 K. (**B**) ^{15}N α-70^{Gly} MoFe protein at τ as indicated. *Conditions*: microwave frequency, 34.806 GHz; $g = 3.6$; 10−40 scans; T = 2 K.

signals with small couplings. These spectra were taken at g_1, where one can observe a single-crystal-like ENDOR spectrum, and g_2, where the EPR and ENDOR intensities are the greatest; Figure 4B shows the spectra collected at g_2 for $500 \leq \tau \leq 900$ ns. No additional signal is observed in these spectra with smaller hyperfine coupling than that of ^{15}N2, and the same is true for spectra collected at g_1. Our

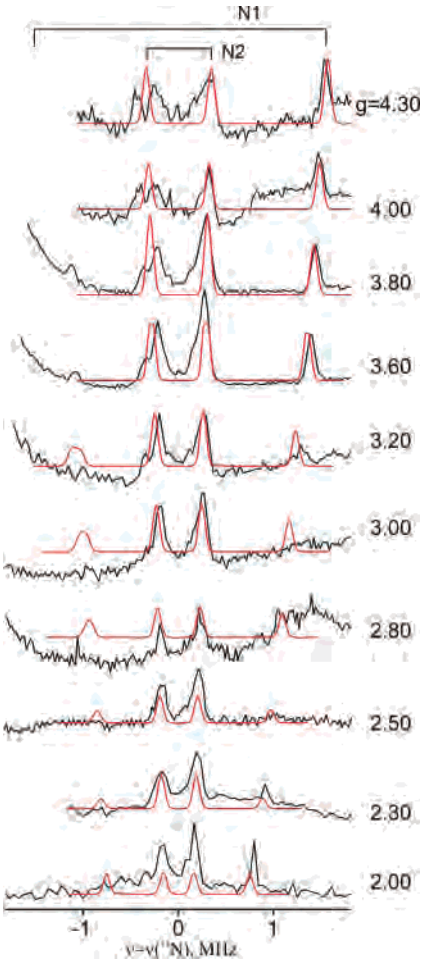

Figure 5. The field dependence of ^{15}N Mims ENDOR lines for ^{15}N uniformly labeled α-70^{Gly} MoFe protein. The strongly coupled nitrogen signals are obscured by Mims "blind spots" at ±1 MHz. Conditions: microwave frequency, 34.785 GHz; Mims sequence, $\pi/2 = 52$ ns, $\tau = 500$ ns; RF = 20 μs; 100 shots/point; repetition time, 5 ms; temperature, 2 K. Simulation (red) parameters: $g = [4.49, 3.62, 2.00]$; hyperfine tensors $^{3/2}A_1 = [1.45, 1.5, 1.5]$ MHz; $^{3/2}A_2 = [0.32, 0.32, 0.32]$ MHz. Note: As discussed in the text, the signal from N2 in fact represents an overlap of responses from two conformers. No effort was made to reproduce the effects of their slight inequivalence; the simulations are primarily presented to show that the couplings are indeed essentially isotropic.

long experience with ^{15}N ENDOR[45] has shown that such spectra readily reveal signals with an observed splitting of $A \sim 0.1$ MHz or less. In spectra taken at fields in the vicinity of $g_{2,3}$, this would correspond to an upper limit to the intrinsic couplings, $^{3/2}\boldsymbol{A}(^{15}\mathrm{N_X}; g_2) \leq 0.05$ MHz (eq 3).

^{14}N ENDOR. The ^{14}N ESEEM and ^{15}N ENDOR analyses of MoFe protein imply that there are only two types of hyperfine-coupled $^{14/15}$N, but preliminary ^{14}N ENDOR observations led to the suggestion that there might be three or four types of ^{14}N.[16] To resolve this possible discrepancy, we generated and analyzed 2D field-frequency plots of ^{14}N Mims pulsed ENDOR spectra for MoFe protein (Figure S2, Supporting Information)). These measurements confirm that the (i) 35 GHz pulsed ^{15}N ENDOR signals observed for (^{15}N)MoFe protein, (ii) the ^{14}N signals observed by X-band ESEEM, and (iii) the 35 GHz pulsed ^{14}N ENDOR signals

(45) Tierney, D. L.; Martásek, P.; Doan, P. E.; Masters, B. S.; Hoffman, B. M. *J. Am. Chem. Soc.* **1998**, *120*, 2983−2984.

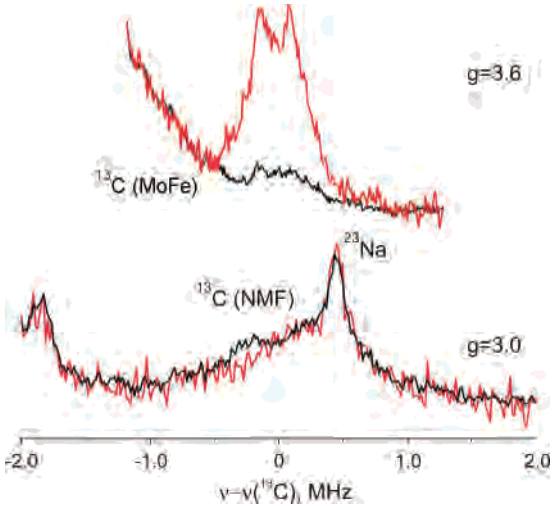

Figure 6. ENDOR spectra. (upper traces) Comparison of pulsed ^{13}C ENDOR spectra for ^{13}C 6% MoFe WT protein (red) vs MoFe WT protein with natural abundance 1.1% of ^{13}C (black). Conditions: Mims sequence; $\pi/2 = 52$ ns, $\tau = 500$ ns, RF = 10 μs, 30 shots/point, 10 ms repetition rate, 2 K, $g = 3.60$, (^{13}C-labeled) 34.690 GHz, 36 scans, and (nonlabeled) 34.702 GHz, 41 scans. (lower traces) Comparison of pulsed ^{13}C ENDOR spectra for ^{13}C 6% enriched FeMo-co extracted in NMF (red) vs FeMo-co with natural abundance 1.1% of ^{13}C (black). The sharp line at +0.45 MHz arises from a Na impurity (see the Supporting Information). All spectra (upper and lower) were normalized to the number of scans and to the echo intensity, so the ratio of intensities of ENDOR lines for different samples reflects the ratio of ^{13}C concentrations. Conditions: Mims sequence; $\pi/2 = 52$ ns, $\tau =$ 500 ns, RF = 10 μs, 30 shots/point, 2 K, $g = 3.00$, (^{13}C-labeled) 34.690 GHz, 10 ms repetition rate, 278 scans, and (nonlabeled) 34.702 GHz, 10 ms repetition rate, 139 scans.

all are associated with the same two sites, N1 and N2. As the correction of a tentative assignment of an additional feature, which now has been found to be from natural-abundance ^{13}C (Figure S2), there are no ENDOR signals from (^{14}N) WT protein that are not accounted for by ^{14}N1 and ^{14}N2.

3.4. ^{13}C (and ^{23}Na) ENDOR. To test the possibility that **X** = C, pulsed ENDOR spectra have been collected from MoFe with ^{13}C in natural abundance (1.1%) and from a sample enriched to 6% ^{13}C ('(^{13}C)MoFe'). Figure 6 (upper) shows spectra obtained at $g = 3.6$, which corresponds to the g_2 maximum of the EPR signal. The natural-abundance sample shows a weak, narrow (<1 MHz broad) feature centered at the ^{13}C Larmor frequency. This feature is at least 5 times more intense in the enriched protein, confirming that this signal indeed is from ^{13}C. The more intense signal from the enriched sampled is seen to be a doublet, split by an apparent coupling of $A \sim 0.25$ MHz, perhaps with shoulders corresponding to $A \sim 0.7$ MHz. Broader radio frequency (RF) scans showed no additional signals that correspond to ^{13}C with larger coupling.

The $g = 3.0$ ^{13}C ENDOR spectra of the ($^{12/13}$C)FeMo-co isotopomers extracted into NMF are presented in Figure 6 (lower). The spectra from both the natural-abundance and enriched FeMo-co exhibit a signal centered at the ^{13}C Larmor frequency. However, in this case the intensities of the ^{13}C-enriched and natural-abundance samples are the same. Hence, we may conclude that these are not associated with **X** = C *or* with carbons of homocitrate and instead must be associated with the natural-abundance ^{13}C of NMF. These observations indicate that if **X** = C, then its ^{13}C hyperfine coupling

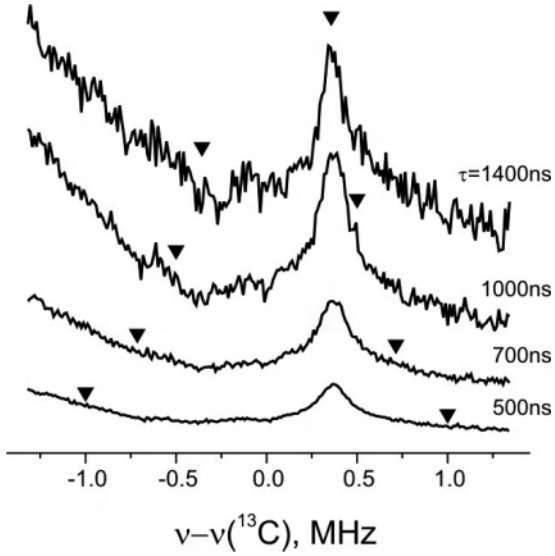

Figure 7. τ dependence of ENDOR spectra of ^{13}C 6% FeMo-co extracted in NMF shows that the +0.35 MHz line does not come from ^{13}C nuclei. The triangles represent the Mims "blind spots" for $A(^{13}C) = 0.7$ MHz (see eq 1). Conditions: microwave frequency, 34.695GHz; $g = 3.6$; Mims sequence, $\pi/2 = 52$ ns, $\tau = 500-1400$ ns; RF = 10 μs; 50 shots/point; repetition time, 10 ms; 15−65 scans; temperature, 2 K.

is too small to have given significant intensity in the spectra collected. Given the ready detection upon enrichment of the signal with $A \sim 0.25$ MHz, we suggest that if **X** = C, then the upper limit on the observed coupling near g_2 again must be, $A(^{13}C_X) \leq 0.1$ MHz, corresponding to $^{3/2}\mathbf{A}(^{13}C_X; g_2) \leq$ 0.05 MHz.

The spectrum of FeMo-co in NMF shows an additional sharp signal offset from the ^{13}C Larmor frequency by ~0.45 MHz (at $g_2 = 3.6$) that is not present in the spectrum of the enzyme.[16,17] The intensity of this signal is unchanged by ^{13}C enrichment; hence, it cannot be from a ^{13}C associated with FeMo-co. As this peak falls at the Larmor frequency of ^{23}-Na, we previously suggested it might be from Na^+ ions in solution that interact with the dissolved FeMo-co, but an alternate assignment would be as the ν_+ feature of a doublet from natural-abundance ^{13}C of NMF, with $A = 0.7$ MHz but unequal intensities for ν_+ and ν_-. To establish the identity of this peak, we examined it as a function of the interval, τ, between the first and second pulses of the Mims ENDOR sequence. If this peak is associated with a ^{13}C having $A =$ 0.7 MHz, then according to eq 1, it should be nulled in a spectrum collected with the pulse interval $\tau = 1/A = 1.4$ μs, but Figure 7 shows that this is not the case. Moreover, the magnetic field dependence of this peak corresponds to the Larmor frequency of ^{23}Na. Finally, if this line were part of a ^{13}C doublet, one would also expect its hyperfine coupling to increase as the observing magnetic field is decreased within the EPR envelope of the $S = {}^3/_2$ FeMo-co (eq 3); this also is not the case (Figure S3, Supporting Information). Thus, the cofactor in NMF in fact shows a "distant-ENDOR" signal from ^{23}Na dissolved in the NMF.

4. DFT Calculations

4.1. Geometry Comparisons for X = C/N/O. Tables 2 and 3 below show that, when comparing optimized FeMo-

Table 2. Analysis of the FeMo-co Core Geometry for the Optimized **X** = C/N/O Alternatives, BS7 Spin Coupling. Maximum (max), Mean, and Root-Mean-Square (rmsd) Deviations from the 1M1N X-ray Structure

	Interatomic distances deviations (Å) to 1M1N X-ray structure					
	Fe−**X** (6 distances)			all bonding within [Mo-7Fe-9S-**X**] (30 distances)		
X	max	mean	rmsd	max	mean	rmsd
C	−0.06	−0.01	0.04	0.08	0.01	0.04
N	0.05	0.01	0.04	−0.09	0.00	0.04
O	0.16	0.09	0.10	0.16	0.03	0.06

Table 3. [6Fe] Prismane Fe−**X** Bonding Distances Optimized for **X** = C/N/O Alternatives, BS7 Spin Coupling, Compared to the Corresponding Values from the 1M1N X-ray Structure

	Fe−X (Å)			
Fe of [6Fe]	**X** = C	**X** = N	**X** = O	exptl
2	1.99	1.99	2.11	1.99
3	1.99	1.95	2.03	1.95
4	2.00	2.01	2.12	1.96
5	1.99	1.99	2.10	2.03
6	2.00	2.00	2.14	2.05
7	2.00	1.97	2.07	2.01

co structures for **X** = $C^{4-}/N^{3-}/O^{2-}$ anion alternatives to 1M1N PDB (1.16 Å resolution),[3] the **X** = C and **X** = N candidates perform better than **X** = O. In particular, the prismane Fe−**X** distances are on average ∼0.1 Å too long for **X** = O, whereas the average discrepancy is 0.01 Å only for **X** = C (contraction) and **X** = N (expansion). The present results disfavoring **X** = O as the FeMo-co interstitial atom are in line with those previously obtained, although the DFT functional used here (PW91) is different from those we[6] (BP86) and others[18] (revPBE) have applied to FeMo-co before. The interplay between the charge and size of **X** anion is clearly critical for its ability to fit the structural parameters of the [6Fe] prismane: C^{4-} is able to contract Fe−**X** more efficiently than N^{3-}, but C^{4-} is bulkier than N^{3-}. An earlier calculation with an empty central cavity showed that the Fe−Fe distances across the central "waist" of the cofactor were about 0.15 Å larger than experiment, although other features of the optimized geometry were in acceptable agreement with experiment.[6,37] Overall, the present and previous structures for the [Mo-7Fe-9S-**X**] core indicate that **X** = O and **X** = vacant are in poorer geometric agreement with the X-ray structure than are **X** = N and **X** =C.

4.2. Hyperfine Coupling to the Central Atom. We report here the first attempt to calculate the central **X** hyperfine signal using DFT in combination with the BS approach for spin coupling. The plausible oxidation states assignment [$Mo^{4+}3Fe^{3+}4Fe^{2+}$] for the metals[6,7,29] leads to 10 possible simple spin-coupling modes of the iron sites designated BS1 to BS10 (see the Computational Details section).[37] We previously found BS6 as the ground-state spin coupling for **X** = vacant, with BS7 or BS2 as slightly higher energy states.[37] Using the PW91 DFT functional, we now find that for **X** = N, BS7 is the predicted ground state, with BS6 as the first excited state, which is consistent with other DFT studies.[13,14] Systematic consideration of the interstitial atom hyperfine signal for **X** = N at all the BS alternatives reveals a striking dependence on the spin coupling (Table 4). BS states numbers 1, 2, 4, 5, 7, and 8, which display overall three spin-up and three spin-down (3↑:3↓) pattern for the [6Fe] iron prismane sites, show weak $N_{\mathbf{X}}$ hyperfine coupling: $0.1 \le a_{iso}(^{14}N_{\mathbf{X}}) \le 1.9$ MHz; (absolute $a_{iso}(\mathbf{X})$ values are discussed in the text; their signs are given in Table 4.). In contrast, the remaining four BS states, 3, 6, 9, and 10, which all display 4↑:2↓ spin pattern within [6Fe], produce much larger hyperfine interactions for **X**, with $7.8 \le a_{iso}(^{14}N_{\mathbf{X}}) \le 11.4$ MHz. For the two lowest-energy states BS7 (≡0.0 kcal/mol, 3↑:3↓) and BS6 (+6.6 kcal/mol, 4↑:2↓), calculated $a_{iso}(^{14}N_{\mathbf{X}})$ values are 0.3 and 9.6 MHz, correspondingly.

Table 4. Calculated Spin-Projected ($P_{\mathbf{X}} = 0.46$) Isotropic Hyperfine Coupling $a_{iso}(\mathbf{X})$, the Total Hyperfine Tensor $A_{tot}(\mathbf{X})$, ρ_s and ρ Net Electron Spin Populations at **X** = ^{14}N Central Ligand (if Not Otherwise Mentioned), and the Corresponding Relative Energies ΔE for Spin Couplings BS1−10 of FeMo-co M^N State

BS state		a_{iso} (MHz)	$^{3/2}\boldsymbol{A}$ (MHz)	$\rho_s(\mathbf{X})$ ($10^{-4}e$)	$\rho(\mathbf{X})$ ($10^{-4}e$)	ΔE (kcal/mol)
1		0.37	[0.04; 0.42; 0.66]	10	69	33.1
2		−0.49	[−0.83; −0.53; −0.12]	−22	334	10.4
3		11.44	[10.34; 11.40; 12.57]	204	−292	23.4
4		−0.18	[−0.43; −0.25; 0.13]	3	5	11.0
5		1.85	[1.16; 1.87; 2.53]	50	157	20.6
6		9.59	[8.58; 9.43; 10.78]	195	−245	6.6
7	**X** = ^{13}C	−0.95	[−2.21; −1.38; 0.73]	−13	59	
	X = ^{14}N	−0.27	[−0.51; −0.38; 0.07]	−6	35	≡0.0
	X = ^{17}O	−0.10	[3.01; 0.05; −3.35]	2	52	
8		0.07	[−0.57; 0.11; 0.67]	−1	102	13.8
9		7.82	[7.00; 8.11; 8.36]	130	−142	21.2
10		8.92	[8.39; 8.65; 9.71]	150	192	12.0

Contrary to previous proposals,[4,6] a small total Mulliken spin population $\rho(\mathbf{X})$ associated with the central ligand ($|\rho(N_{\mathbf{X}})| \le 0.03e$ for any of the BS states (see Table 4) does not necessarily imply a small $a_{iso}(\mathbf{X})$ contribution to the hyperfine coupling. For example, the current result of $\rho(^{14}N_{\mathbf{X}}) = -0.02e$ for BS6 is nearly identical to the results from our previous work[6] and from other groups,[18] yet a large contribution of $a_{iso}(^{14}N_{\mathbf{X}}) = 9.6$ MHz was found for this spin alignment. This is because in a complex spin density distribution field such as the inside area of the [6Fe] cage, Mulliken spin density does not necessarily correspond to the $|\Psi(0)|^2$ point spin density at the position of the nucleus (see eq 4). Only the $\rho_s(\mathbf{X})$ spin populations from s-type orbitals contribute to a_{iso}, and $\rho_s(\mathbf{X})$ is not always the largest contributor to $\rho(\mathbf{X})$ (see Table 4). For the four BS states with the strong coupling of **X** to the FeMo-co spin $S = {}^3/_2$ (4↑:2↓ spin pattern within [6Fe]), $a_{iso}(\mathbf{X})$ displays approximate proportionality to $\rho_s(\mathbf{X})$: $4.9 \times 10^2 < a_{iso}(^{14}N_{\mathbf{X}})/\rho_s(N_{\mathbf{X}}) < 6.0 \times 10^2$ (MHz/e). For the other BS states with the weak **X** coupling (3↑:3↓ spin pattern within [6Fe]), $a_{iso}(\mathbf{X})$ is small and $a_{iso}(^{14}N_{\mathbf{X}})/\rho_s(N_{\mathbf{X}})$ varies significantly, presumably due to the fact that $|\Psi(0)|^2$ is only approximately proportional to $\rho_s(N_{\mathbf{X}})$. The absence of a clear $N_{\mathbf{X}}$ hyperfine signal for the resting-state FeMo-co might thus be due to an effective cancellation of electron spin density contributions from the six prismane irons in a 3↑:3↓ spin coupling (as in BS7, the lowest-energy BS state), which results in a small $|\Psi(0)|^2$ point electron density at the **X** nucleus position.

The BS7 coupling scheme yields $a_{iso}(^{14}N_{\mathbf{X}}) = 0.27$ MHz, $a_{iso}(^{13}C_{\mathbf{X}}) = 1.0$ MHz, and $a_{iso}(^{17}O_{\mathbf{X}}) = 0.1$ MHz for the **X**

= N, C, and O alternatives (Table 4). The computed ^{14}N coupling is 4-fold larger than the experimentally estimated upper bound; the ^{13}C coupling is more than an order of magnitude larger than the estimated bound; ^{17}O labeling is prohibitively expensive. For $^{14/15}$N and ^{13}C, however, uncertainties in the DFT calculations and in our estimates of $P_{\mathbf{X}}$, make it difficult to definitively rule out a possible carbon or nitrogen central atom with a hyperfine coupling less than 0.1 MHz.

4.3. Nuclear Quadrupole Coupling Constants. A putative **X** = N atom would reside in a highly symmetric electrostatic environment, with six nearly equidistant nearest-neighbor iron atoms. Not surprisingly, a small value of $e^2qQ/h = 0.66$ MHz (asymmetry parameter, $\eta = 0.58$) is calculated for the near-symmetrically bonded central ^{14}N. This is much smaller than the values of 2.17 MHz (N1) and 3.5 MHz (N2) obtained from the experiment on MoFe-bound FeMo-co. Unpublished DFT calculations on larger models that include the first shell of protein ligands show quadrupole couplings in the range of 1.6−4.3 MHz for protein nitrogen atoms. These results support the experimental conclusion that the N1 and N2 signals must come from the MoFe protein and not from the FeMo-co-associated central nitrogen.

4.4. Iron Hyperfine Calculations. In Table 1, the calculated semiempirical Fe hyperfine coupling parameters (a_i^{calc}) are compared to the experimentally obtained (a_i^{exp}) values.[29] The spectroscopic sites are matched with the crystallographic sites based on our current calculations and a spin-coupling scheme based on BS7. While the agreement of the semiempirical to experimental values is not perfect, it is reasonably good. One additional measure of the quality of this result is to sum a_{iso} over all the sites, giving a value we have called a_{test}.[40] From Table 1, we find a calculated value of −23.1 MHz, which compares reasonably well with the experimental value of −17.9 MHz. Our overall conclusion is that BS7 is consistent with Fe hyperfine values but that it is not possible to rule out other spin-coupling schemes based just on this information.

5. Discussion

We first discuss the ENDOR/ESEEM evidence regarding the possibility that **X** = N or C that is hyperfine-coupled to the $S = {}^3/_2$ spin system of resting-state FeMo-co and then consider the hyperfine couplings predicted by BS-DFT computations in light of experiment.

5.1. ENDOR/ESEEM Experiments. (a) ^{14,15}N ENDOR/ESEEM of MoFe. Our in-depth ESEEM study of MoFe protein disclosed the presence of two nitrogen atoms, N1 and N2, that interact with the $S = {}^3/_2$ spin system of FeMo-co. Subsequent 35 GHz ENDOR measurements showed two distinct ^{15}N ENDOR signals from isotopically enriched MoFe protein, which were attributed to N1 and N2. We here report that the hyperfine tensors for these two ^{15}N atoms, as obtained through the analysis of 2D field-frequency plots of the ^{15}N ENDOR spectra taken across the EPR envelope of (^{15}N) FeMo-co in MoFe protein, are consistent with those for ^{14}N1 and ^{14}N2 as determined by ESEEM. This confirms the correlation between ^{14}N ESEEM and ^{15}N ENDOR of FeMo-co in MoFe protein and their assignment to two polypeptide nitrogens, with isotropic hyperfine couplings for ^{15}N1 and ^{15}N2 of $a_{\mathrm{iso}}(^{15}\mathrm{N1/2}) = 1.5/0.3$ MHz, respectively.

Extensive measurements show clearly that there are no ^{15}N atoms that are more strongly coupled. Note that this is true even though the experimentally determined $^{3/2}\mathbf{A}(^{15}\mathrm{N1/2})$ are roughly isotropic, whereas the corresponding tensors computed by DFT have substantial anisotropy (Table 4), which can interfere with detection. First of all, the conversion of the $S = {}^3/_2$ hyperfine tensor to the observed tensor, expressed relative to the fictitious spin $S' = {}^1/_2$, introduces substantial anisotropy even to an isotropic coupling (eq 3). To further test for the consequence of anisotropy on the detection of a putative **X** = N ($\mathrm{N_X}$), we have carried out ENDOR simulations at multiple fields for the isotropic coupling of ^{15}N2 and for $^{15}\mathrm{N_X}$ using the calculated hyperfine tensor of Table 4. These simulations, overlaid in Figure S4 (Supporting Information), show that for some values of the external field the anisotropy would indeed diminish the maximum intensity of the $\mathrm{N_X}$ signal relative to that of the N2 signal but that there are substantial ranges of the field where the intensity of the $\mathrm{N_X}$ signal would be no less than that of the N2 signal. We conclude that the collection of a 2D pattern of spectra taken at fields across the entire envelope of the $S = {}^3/_2$ signal from MoFe ensures that the detection of $^{15}\mathrm{N_X}$ is *not* being compromised by anisotropy of the $^{15}\mathrm{N_X}$ hyperfine tensor.

A second possible difficulty with these measurements is that the signal in low-temperature experiments might be broadened by static disorder. **X** is not precisely centered in the experimental and the calculated structures (Table 3) and might adopt multiple locations relative to the [6Fe] cage, each with a slightly different hyperfine coupling, and this would broaden the spectrum. However, the minor conformational heterogeneity revealed in Figure 5 does not compromise the ability to detect the ^{15}N ENDOR signals from N1, and the smaller the coupling the less likely it is that broadening by a fraction of the coupling would have a seriously deleterious effect. Thus, we dismiss this issue, although it will nonetheless be addressed by future DFT computations which might quantify any hyperfine dispersion that might arise.

While keeping in mind the above caveat, the ^{15}N ENDOR results can only be interpreted at this time as indicating that if **X** = N, then at any field examined, $A(^{15}\mathrm{N_X})$ is so much less than $A(^{15}\mathrm{N2})$ that the signal from $^{15}\mathrm{N_X}$ cannot be detected. Given the good S/N ratio and resolution of the signals from N2, we suggest that these results are compatible with **X** = N only if at fields in the vicinity of $g_{2,3}$, the upper limit to the intrinsic couplings, $^{3/2}\boldsymbol{A}(^{15}\mathrm{N_X}; g_{2,3}) \leq 0.05$ MHz (eq 3), leading us to estimate that $a_{\mathrm{iso}}(^{15}\mathrm{N_X}) \leq 0.05-0.1$ MHz or $a_{\mathrm{iso}}(^{14}\mathrm{N_X}) < 0.03-0.07$ MHz.

Our earlier experimental work had suggested that there might be ^{14}N signals seen with the WT protein that are not accounted for by N1 and N2. We therefore re-examined the 35 GHz pulsed ^{14}N ENDOR signals of natural-abundance MoFe protein. We find that there are in fact no ^{14}N signals

seen with WT protein that are not accounted for by N1 and N2; the ^{15}N ENDOR signals observed for (^{15}N)MoFe protein and the ^{14}N signals observed both by ESEEM[15,44] and now by pulsed ENDOR are associated with the same two sites, N1 and N2. With the corrected assignment of an additional feature to natural-abundance ^{13}C, there are indeed neither ^{15}N nor ^{14}N signals seen with WT protein that are not accounted for by N1 and N2.

^{14,15}N ENDOR/ESEEM of FeMo-co in NifX and NMF. We find that (^{14}N)FeMo-co in NifX and in NMF both show well-resolved ESEEM signals, from ^{14}N in the former and possibly from ^{14}N and ^{23}Na in the latter. The echo modulation and frequency-domain spectra are very different in the two samples (Figures 3 and 6), but in both cases the results are unchanged for (^{15}N)FeMo-co. Thus, in both environments the nuclei that are coupled to the electron spin must be associated with the FeMo-co surroundings, NifX, or NMF and not with $\mathbf{X} = {}^{14}$N. On the basis of the S/N ratio of our measurements, we conclude that if $\mathbf{X} =$ N, then it must give rise to ^{14}N ESEEM with a modulation amplitude of $<2\%$.

To test these results against predictions based on the DFT computations, we computed ESEEM timewaves for a field corresponding to g_2, for a ^{14}N signal with the hyperfine and quadrupole parameters obtained from the DFT calculations for $S = {}^3/_2$ FeMo-co with $\mathbf{X} = {}^{14}$N, ${}^{3/2}\mathbf{A} = [\,-0.51, -0.38, 0.07\,]$ MHz (BS7, Table 4), the modest nuclear quadrupole coupling constant given above of $e^2qQ = 0.7$ MHz, reflective of the high-symmetry environment, and asymmetry parameter of $\eta = 0.6$; the calculation was repeated for a wide range of assumed orientations of **A** and quadrupole tensor relative to **g**. These computations give modulation depths of $\sim$6%, compared with the upper limit of $\sim$2% permitted by experiment.

The ESEEM results further and decisively validate the results of ^{15}N pulsed ENDOR measurements on extracted cofactor. The occurrence of sharp frequency-domain features in the ^{14}N ESEEM patterns from FeMo-co in NifX and NMF (Figures 2 and 3) shows that the distribution of substates associated with the inhomogeneous broadening of the EPR signals from these systems (Figure 1) does *not* give rise to a corresponding distribution in hyperfine couplings that could broaden ^{15}N ENDOR signals from (^{15}N)FeMo-co in these environments, perhaps making it undetectable.

The 35 GHz Mims ENDOR spectra of (^{15}N)FeMo-co in NifX or NMF show no ^{15}N signals when taken under conditions equivalent to those used to yield the well-defined ^{15}N spectra from (^{15}N)FeMo-co in MoFe (Figure 4). However, a ^{14}N ENDOR signal is detected from the NifX polypeptide and ENDOR signals from ^{13}C of NMF and ionic ^{23}Na. Thus, the extracted (^{15}N)FeMo-co shows ENDOR signals from its NifX and NMF environments but not from a putative $\mathbf{X} = {}^{15}$N, under conditions where ^{15}N ENDOR signals are seen from ^{15}N1/2 of the MoFe environment.

^{13}C. ENDOR spectra from FeMo-co in MoFe protein and in NMF display signals centered at the ^{13}C Larmor frequency, from weakly coupled ^{13}C nuclei with $A \sim 0.25$ MHz (and possibly $\sim$0.7 MHz). When MoFe is $\sim$5-fold enriched in ^{13}C, the intensity of the signal obtained from the FeMo-co in the protein increases correspondingly, but that obtained from isolated FeMo-co in NMF does not. Thus, the ^{13}C ENDOR signal comes neither from $\mathbf{X} =$ C *nor* from homocitrate of the cofactor but from the surroundings of FeMo-co, the MoFe polypeptide in the case of the MoFe protein and NMF itself for the extracted cofactor. We estimate further that if $\mathbf{X} =$ C, then the upper limit to the observed coupling near $g_{2,3}$ again must be $A({}^{13}\mathrm{C}_\mathbf{X}) \leq 0.1$ MHz, corresponding to ${}^{3/2}\boldsymbol{A}({}^{13}\mathrm{C}_\mathbf{X}; g_{2,3}) \leq 0.05$ MHz; overall, we estimate $a_{iso}({}^{13}\mathrm{C}_\mathbf{X}) \leq 0.05-0.1$ MHz. The absence of a signal from homocitrate supports our original assignment of a nonmagnetic ($S = 0$) Mo(IV).

5.2. DFT Computations. The computations for the two lowest-energy states, BS7 ($\equiv$0.0 kcal/mol, 3$\uparrow$:3$\downarrow$) and BS6 (+6.6 kcal/mol, 4$\uparrow$:2$\downarrow$), give isotropic couplings for $\mathbf{X} =$ N of $a_{iso}({}^{15}\mathrm{N}_\mathbf{X}) = 0.4$ and 13.7 MHz, respectively. Thus, if $\mathbf{X} =$ N, experiment categorically rules out BS6. The predicted value of $a_{iso}({}^{15}\mathrm{N}_\mathbf{X}) = 0.4$ MHz for BS7 is *larger* than that observed for N2, $a_{iso}({}^{15}\mathrm{N2}) = 0.3$ MHz and also larger than the upper bound for $a_{iso}({}^{15}\mathrm{N}_\mathbf{X})$ from the experiment. The uncertainty of the DFT calculations on the **X** hyperfine signal is difficult to estimate. The performance of quantum chemical methods on hyperfine coupling constants has been benchmarked mainly for light main-group radicals with $a_{iso} \sim 10-100$ MHz. Even for systems not involving transition ions, a 10−15% deviation of DFT from the well-established experimental a_{iso} value is considered as a good result.[46] Less is known about DFT performance for the main-group elements in transition-metal complexes or enzyme active sites with paramagnetic metal centers. Qualitatively good results have been obtained in several instances.[47−49] In addition to the uncertainties inherent in DFT, we also have to estimate the scaling factor $P_\mathbf{X}$, which has its own uncertainties, as discussed above. Hence, it is certainly possible that the actual hyperfine coupling for **X** is several tenths of a megahertz lower than our best DFT estimate and may approach zero.

6. Conclusions

The identity of the central atom in FeMo-co has been of intense interest since its existence was first reported. Through the joining of experiment and computations, the present report presents the following conclusions:

(1) ENDOR/ESEEM experiments on $S = {}^3/_2$ FeMo-co in the MoFe protein itself, in the NifX protein, and in NMF solution show no signals that can be assigned to $\mathbf{X} =$ N or C; all ^{14,15}N ENDOR signals from FeMo-co incorporated in MoFe are self-consistently assigned to two polypeptide nitrogens, N1 and N2.

(2) Analysis of the measurements suggests that if $\mathbf{X} =$ N, then at all fields of measurement it must give an observed

(46) *Calculation of NMR AND EPR Parameters: Theory and Applications*; Kaupp, M., Buehl, M., Malkin, V. G., Eds.; Wiley-VCH: Weinheim, Germany, 2004.
(47) Han, W.-G.; Liu, T.; Lovell, T.; Noodleman, L. *J. Am. Chem. Soc.* **2005**, *127*, 15778−15790.
(48) Sinnecker, S.; Neese, F.; Noodleman, L.; Lubitz, W. *J. Am. Chem. Soc.* **2004**, *126*, 2613−2622.
(49) Kuramochi, H.; Noodleman, L.; Case, D. A. *J. Am. Chem. Soc.* **1997**, *119*, 11442−11451.

splitting $A(^{15}N_X) < 0.1$ MHz, corresponding to $A(^{14}N_X) < 0.05$ MHz. This conclusion is compatible with $\mathbf{X} = N$ only if $a_{iso}(^{15}N_X) < 0.05-0.1$ MHz and $a_{iso}(^{14}N_X) < 0.03-0.07$ MHz.

(3) ^{14}N ESEEM measurements of ($^{14/15}N$)FeMo-co extracted into NMF and incorporated into the carrier protein NifX show modulation from ^{14}N of the surroundings but none from a hyperfine-coupled $\mathbf{X} = {}^{14}N$.

(4) However, the ESEEM results validate the ^{15}N ENDOR measurements from FeMo-co extracted into NMF or incorporated into NifX, in that the sharp frequency-domain features in the ^{14}N ESEEM patterns from FeMo-co in NifX and NMF (Figures 2 and 3) show that the absence of 35 GHz ENDOR signals from $\mathbf{X} = {}^{15}N$ is not ascribable to a distribution-broadening of the ^{15}N ENDOR signals from (^{15}N)FeMo-co in these environments.

(5) The ^{13}C ENDOR spectra of natural-abundance FeMo-co in MoFe and extracted into NMF both show ^{13}C signals. These have appropriately enhanced intensity in spectra of MoFe protein that is ^{13}C-enriched, but are not enhanced in the spectra of extracted FeMo-co. Thus, these signals are not associated with $\mathbf{X} = C$ or with homocitrate: We estimate that these results are compatible with $\mathbf{X} = C$ only if $a_{iso}(^{13}C_X) < 0.05-0.1$ MHz.

(6) The first DFT calculations of the hyperfine constants for **X** predict that hyperfine couplings to **X** in the computed (BS7) ground state are small because there is a balance of nearly equal and canceling contributions from neighboring spin-up and spin-down iron atoms.

(7) If $\mathbf{X} = C/N$, then the decoupling required by experiments strongly supports the currently preferred BS7 spin-coupling scheme, and it rules out the BS6 assignment suggested earlier. The computed geometry and iron hyperfine and Mössbauer isomer shift data are also in good accord with a BS7 spin assignment and an N or C central atom.

(8) Comparison with the experimentally estimated limits for the hyperfine couplings indicates that the BS7 couplings computed for $\mathbf{X} = N/C$ by BS-DFT still are easily large enough (Table 4) to have led to observable signals.

(9) While this result inevitably focuses attention on the possibility that $\mathbf{X} = O$ and on the even higher resolution X-ray structural measurements to confirm the presence of **X**, it is likewise clear that uncertainties in the current calculations mean that very small (<0.1 MHz) couplings cannot be ruled out: **X** might indeed be magnetically decoupled from the resting FeMo-co electron spin system.

In summary, interlocking and mutually supportive experiments with multiple spectroscopies on FeMo-co isotopomers in multiple environments provide powerful evidence that $\mathbf{X} \neq N/C$, unless **X** in effect is magnetically decoupled from the $S = {}^3/_2$ electron spin system of resting FeMo-co. Clearly, even the 'simple' task of identifying **X** presents one of the many hurdles in the path toward a mechanism of nitrogenase function.

Acknowledgment. NIH Grant Nos. R01-GM59087 to L.C.S. and D.R.D. and GM39914 to D.A.C. and L.N.; NSF Grant No. MCB0723330 to B.M.H.

Supporting Information Available: Figures S1−S4 in PDF format. This material is available free of charge via the Internet at http://pubs.acs.org.

IC7018814